Functionally Relevant Electric-Field Induced Perturbations of the Prosthetic Group of Yeast Ferrocytochrome *c* Mutants Obtained from a Vibronic Analysis of Low-Temperature Absorption Spectra

Reinhard Schweitzer-Stenner,*,† Matteo Levantino,‡ Antonio Cupane,‡ Carmichael Wallace,§ Monique Laberge,|| and Qing Huang†

Department of Chemistry, Drexel University, 3141 Chestnut Street, Philadelphia, Pennsylvania 19026, CNISM and Department of Physical and Astronomical Sciences, University of Palermo, Via Archirafi 36, 90123 Palermo, Italy, Department of Biochemistry and Molecular Biology, Dalhousie University, Nova Scotia, Canada B3H 4H7, and Department of Biochemistry and Biophysics and Johnson Research Foundation, University of Pennsylvania Medical Center, Philadelphia, Pennsylvania 19104-6059

Received: February 5, 2006; In Final Form: April 5, 2006

We have measured the low temperature ($T = 20$ K) absorption spectra of the N52A, N52V, N52I, Y67F, and N52AY67F mutants of ferrous *Saccharomyces cerevisiae* (baker's yeast) cytochrome *c*. All the bands in the Q_0- and Q_v-band region are split, and the intensity distributions among the split bands are highly asymmetric. The spectra were analyzed by a decomposition into Voigtian profiles. The spectral parameters thus obtained were further analyzed in terms of the vibronic coupling model of Schweitzer-Stenner and Bigman (Schweitzer-Stenner, R.; Bigman, D. *J. Phys. Chem. B* **2001**, 7064−7073) to identify parameters related to electronic and vibronic perturbations of the heme macrocycle. We report that the electronic perturbation is of B_{1g} symmetry and reflects the heterogeneity of the electric field at the heme, that is, the difference between the gradients along the perpendicular N−Fe−N axis of the heme core. We found that all the investigated mutations substantially increase this electronic perturbation, so that the spectral properties become similar to those of horse heart cytochrome *c*. Moreover, the electronic perturbation was found to correlate nonlinearly with the enthalpy changes associated with the reduction of the heme iron. Group theoretical arguments are invoked to propose a simple model which explains how a perturbation of the obtained symmetry can stabilize the reduced state of the heme iron. Finally, vibronic coupling parameters obtained from the analysis of the Q_v-band region suggest that the investigated mutations decrease the nonplanar deformations of the heme group. This finding was reproduced by a normal mode structural decomposition (NSD) analysis of the N52V and N52VY67F heme conformations obtained from a 1 ns molecular dynamics simulation. We argue that the reduced nonplanarity contributes to the stabilization of the reduced state.

Introduction

It is now well established that the structure and function of the chromophore in heme proteins are modulated by the internal electric field generated by the ionizable and polar side chains of the protein environment.[1−6] This is particularly the case for heme proteins such as cytochrome *c*, which belongs to an important class of redox active proteins.[7] It has a comparatively high redox potential, which is generally thought to be predominantly due to the sulfur atom of the sixth methionine ligand,[8] but the interaction between the internal electric field and the heme is also recognized as an important factor.[9] Theoretical studies on the relationship between redox potential and the charge distribution in the heme cavity have been reported in the literature,[9−11] but they were predominantly aimed at understanding the physical origin of the Gibbs energy changes and the reorganization energy associated with the charge-transfer process. However, the role of the chromophore's electronic structure and its modulation by electrostatic forces is not yet well understood.

The influence of the electric field and other types of heme-protein interactions affecting the symmetry of the heme macrocycle can be probed by spectroscopic techniques. Sutherland and Klein, by means of magnetic dichroism measurements,[12] observed a ca. 120 cm^{-1} splitting of the Q band of horse heart ferrocytochrome *c* at low cryogenic temperatures, which was later found to be mirrored by the resonance Raman excitation profile of the ν_{15} mode.[13] The physical reason for this splitting has subsequently been investigated further by absorption and resonance Raman spectroscopy. What these studies,[14−20] described in more detail by Levantino et al.,[21] have in common is that they invoke symmetry lowering perturbations induced by the protein environment, but a detailed assessment is still lacking. An investigation specifically aimed at determining the influence of the internal electric field on the ferrocytochrome *c* heme group was recently carried out by Vanderkooi and collaborators.[2,3,5] Manas et al.,[2] for instance, measured the Q-band spectra of horse heart (hhc), beef, porcine, tuna (thc), chicken, and yeast cytochrome *c* (yc) at cryogenic temperature.

* To whom correspondence should be addressed. E-mail: rschweitzer-stenner@drexel.edu. Phone: 215-895-2268. Fax: 215-895-1265.
† Drexel University.
‡ University of Palermo.
§ Dalhousie University.
|| University of Pennsylvania Medical Center.

10.1021/jp060755d CCC: $33.50
Published on Web 05/25/2006

Electrostatic and quantum mechanical calculations led them to conclude that the observed band splitting results predominantly from the electric field in the heme cavity.

We have recently carried out a detailed low-temperature absorption study of the Q-band region of hhc and yc.[21] A vibronic analysis of the Q-band spectra based on recorded resonance Raman spectra was performed and showed that a selfconsistent description of the observed splitting and asymmetry of the Q_0 and the Q_v bands of the vibronic sideband requires the consideration of electronic as well as vibronic perturbations, as theoretically predicted by Schweitzer-Stenner and Bigman.[22] The electronic perturbation can be directly inferred from the ratio of the dipole moments associated with the transitions into the split Q_x and Q_y states. It was shown to most likely reflect the gradient inhomogeneity of the internal electric field at the heme (i.e., different gradients along the two perpendicular N−Fe−N heme axes), which gives rise to an additional electronic coupling of B_{1g} symmetry.[3] This perturbation was found to be substantially larger for hhc (95 cm^{-1}) than for yc (50 cm^{-1}). This indeed reflects the difference between the respective electric field gradients, as shown by Laberge et al.[4] The vibronic perturbation parameters indicate that the heme group in yc is more nonplanar and more distorted along a B_{2g} coordinate than in hhc.[21]

In the current study, we apply our experimental and theoretical protocol to mutants of yc. We selected two residues for replacement, namely N52 and Y67. Both residues, via their respective polar CO and OH groups, are incorporated in a hydrogen-bonding network of water molecules which shields the heme group from the dipoles in its environment, thus stabilizing the ferrous, reduced state of the heme iron.[23] Substitutions of N52 by aliphatic residues such as alanine, valine, and isoleucine eliminate the dipole moment associated with its amide side chain and causes a reorganization of the hydrogen-bonding network. They all lower the redox potential, thus favoring the oxidized state. Interestingly, this is predominantly associated with a positive entropic contribution to the respective Gibbs energy rather than with enthalpic changes, which all favor the reduced state.[23] It is reasonable to assume that the positive ΔS reflects a larger conformational flexibility. Thus, all these mutations make yc more similar to hhc, which has a much lower redox potential and exhibits more conformational heterogeneity. If there is a correlation between conformational flexibility, internal field gradient, and electronic heme perturbation as our previous study on hhc and yc suggests, one would expect that the N52 mutations all cause an increase of the B_{1g}-type electronic perturbation. We tested this prediction by measuring and analyzing the low-temperature Q-band absorption of N52A, N52V, and N52I. As for Y67, we investigated the Y67F mutation. In the wild-type protein, the hydroxyl group of Y67 is hydrogen-bonded to the SD atom of M80 which provides the sixth heme ligand. This hydrogen bond affects the electron-withdrawing power of M80.[24] Its substitution by a purely hydrophobic phenylalanine causes a substantial decrease of the redox potential driven by entropic changes. Finally, we investigated the double mutation N52VY67F, which differs from the other mutations in that it stabilizes the oxidized state enthalpically.[23] In this paper, we focus on how the above mutations modify the electronic perturbation of the heme, whereas vibronic perturbations are only briefly discussed. These will be dealt with in the context of a detailed analysis of resonance Raman depolarization ratios, which will be reported in a future publication.

Theoretical Background

The underlying theory of our analysis has been described in general terms by Schweitzer-Stenner and Bigman[22] and in more specific terms (for the analysis of experimental spectra) by Levantino et al.[21] in earlier publications. Here, we solely summarize the definition of the used quantum mechanical parameters.

Electronic Perturbations. The asymmetric protein environment and to a minor extent the peripheral substituents create a perturbing potential at the heme, which can be described in terms of electronic coupling between the excited electronic heme states of the four-orbital model:

$$\delta^{\Gamma}_{Q_l B_m} = \langle Q^0_l | V^{\Gamma} | B^0_m \rangle \tag{1}$$

where V^{Γ} denotes a perturbing potential of symmetry $\Gamma = B_{1g}$, B_{2g}, and A_{2g} under the D_{4h} point group and $|Q^0_l\rangle$, $|B^0_m\rangle$ ($l, m = x, y$) are the state vectors of the two lowest excited electronic heme macrocycle states, which exhibit E_u symmetry in the unperturbed state and can be identified with the 50:50 states of Gouterman's four-orbital model.[25] Adopting the terminology of Zgierski and Pawlikowski,[16] we term $\delta^{\Gamma}_{Q_l B_m}$ an electronic perturbation. As indicated by eq 1, it mixes the components of the excited states, which causes a splitting of the optical bands and a redistribution of the respective oscillator strengths. It is equivalent to the crystal-field perturbation which Canters and co-workers invoked to explain the band splitting of metalloporphyrins in anisotropic matrixes.[26]

As outlined by Levantino et al.,[21] we neglect perturbations of B_{2g} and A_{2g} symmetry, which combined could also contribute to splitting and band intensity redistribution.

Vibronic Perturbations. The vibronic coupling parameter $c^{\Gamma''}_{es}(j)$ denotes the vibronic coupling matrix elements of the jth vibrational mode of the heme macrocycle. In the presence of vibronic perturbations they are written as[16,17]

$$c^{\Gamma''}_{es}(j) = \left\langle e \left| \frac{\partial H_{el}}{\partial q^{\Gamma'}_j} \right| s \right\rangle q^{\Gamma'}_j + \sum_{\tilde{\Gamma}} \chi^{\tilde{\Gamma}}_{es}(j) \tag{2}$$

where

$$\chi^{\tilde{\Gamma}}_{es}(j) = \left\langle e \left| \frac{\partial V^{\Gamma}}{q^{\Gamma'}_j} \right| s \right\rangle q^{\Gamma'}_j$$

The first term describes the vibronic coupling of the jth mode of symmetry Γ' for an ideal D_{4h} symmetry, whereas the second term reflects additional vibronic coupling due to the vibronic perturbations which adds a symmetry $\tilde{\Gamma} = \Gamma \otimes \Gamma'$ to the vibronic coupling term. The vibronic perturbation, which has first been introduced by Zgierski and Pawlikowski,[16] reflects the variation of the perturbing potential by a given molecular vibration. The electronic states $|e\rangle$ and $|s\rangle$ are identified with $|Q^0_x\rangle$, $|Q^0_y\rangle$ and $|B^0_x\rangle$, $|B^0_y\rangle$ of Gouterman's 50:50 state.[25]

Vibronic perturbations modify the Q-band splitting, since $c^{B_{1g}}_{Q_x Q_x} = -c^{B_{1g}}_{Q_y Q_y}$ and $c^{A_{2g}}_{Q_x B_y} = -c^{A_{2g}}_{QB}$. However, depending on the sign of the coupling parameters, the splitting can be reduced or increased.[22] Moreover, vibronic coupling differently affects the apparent transition dipole moments of the x- and y components of vibronic bands. As a consequence, the absorption ratios $R_j = A_{Q_y}(j)/A_{Q_x}(j)$ of the y- and x-component of the jth's mode vibronic sideband differ from each other, while they would be identical in the absence of vibronic perturbations.[22]

Material and Methods

Material. Proteins were prepared by expression of plasmid-borne mutant yeast iso-1-cytochrome *c* (cyc-1) genes in the host *S. cerevisae* GM3C2,[27] which lacks the wild-type gene. Cytochromes were purified, after yeast cell lysis and extraction or precipitation of most other soluble components, by cation-exchange chromatography.[28] In addition to the indicated mutations, all cytochromes thus prepared contain a C102T mutation to ensure that dimerization via disulfide formation does not occur. For the low-temperature absorption measurements, suitable protein amounts were dissolved in a 65% v/v glycerol/water solution containing 0.1 M phosphate buffer at pH 7. The final protein concentration was approximately 5×10^{-6} M. Immediately before the experiments, the proteins were reduced by the addition of 10 mM sodium dithionite and anaerobically transferred to 1 cm-path length metacrylate cuvettes suitable for the measurement of low-temperature optical absorption spectra. For room-temperature absorption and resonance Raman experiments, the protein was dissolved in 0.01 M tris buffer at pH 8 and reduced by a small amount of sodium dithionite. The final concentrations for the absorption and Raman measurements were 5 μM and 0.5 mM, respectively.

Spectroscopy. The set up and the performance of the absorption and Raman measurements have been described in great detail in a recent paper.[21]

Modeling and NSD Calculations. The yeast cytochrome *c* mutant models were prepared using available yeast cytochrome *c* mutated X-ray coordinates at the Research Collaboratory for Structural Bioinformatics (RCSB) data bank, namely 1crh and 1crj.[24] The N52V mutant model was built using InsightII (Accelrys, San Diego) by substituting a Val residue at position 52. Likewise, the Y67F−N52V mutant was generated by additionally substituting a Phe at position 67. The stereochemical quality of the models was verified and corrected using the PROCHECK program.[29] All simulations were performed using CHARMM version c31b2 with the all-atom-27 protein force field included in the distribution[30] and the heme parametrization of Autenrieth et al.[31] The models were equilibrated by subjecting them to 1 ns molecular dynamics (MD) under explicit solvation conditions. After the simulations, the hemes were extracted, and normal structural decomposition calculations were performed using version 2.0 of the NSD program.[19]

Full details of the molecular dynamics protocol and NSD calculations are provided in our recent cytochrome *c* study.[21]

Results and Discussion

The Q_0 bands of all investigated yc mutants measured at $T = 20$ K are displayed in Figure 1b together with the native yc spectrum. Visual inspection immediately reveals that all bands are split into two bands of different intensity assignable to the Q_{0x} and Q_{0y} components of the underlying optical transition. The effect of this splitting and asymmetry is also observed in the vibronic replicas of the Q_v-band region (Figure 1a).

As evident from Figure 1b, a first effect of the investigated mutations is a spectral shift; peak frequency values of the Q_0 band are reported in Table 1. In general, the apolar mutations studied induce a spectral red-shift. The effect increases with increasing the apolar side chain in position 52 and is more pronounced for mutations involving the Y67 position. Analogous red-shifts have been observed for both the Q_0 band and band III (a charge-transfer band occurring at ~760 nm in deoxy-myoglobin and -hemoglobin) as a result of apolar mutations at position E7 in the distal heme pocket of deoxy-myoglobin.[32] Moreover, spectral alterations in the Soret band of deoxy-hemoglobin are also observed following the VE11 → T polar isosteric mutation in the α chains.[33] These effects have been interpreted in terms of an altered polarity of the distal heme pocket (likely involving the presence/absence of a water molecule) causing alterations in the electric field at the chromophore.[32,33] In analogy with the above results, one may suggest that the spectral red-shifts obtained in the present study (Figure 1b) reflect a change of the electrostatic potential at the heme plane induced by the substitution of polar (N52, Y67) by apolar side chains (A, V, I, F). In line with the findings of Blouin and Wallace,[23] this most likely involves the partial or even total disruption of the network of hydrogen-bonded water molecules that characterizes the active site of native yeast cytochrome *c*. In fact, these considerations are in agreement with theoretical results reported by Manas et al.[2] as well as Schweitzer-Stenner and Bigman,[22] who predicted a quadratic Stark effect involving a blue-shift of the Q band due to an increasing electric field. Hence, the observed redshift caused by the apolar mutations indicate a decrease of the internal electric field.

To illustrate our spectral analysis procedure, we refer to the absorption spectrum of the unmodified yc in Figure 2. As already noted, visual inspection immediately reveals that it consists of a series of doublets: the lowest frequency doublet is the Q_0 band split into its Q_{0x} and Q_{0y} components, while the higher frequency doublets are vibronic replicas. To analyze the spectrum quantitatively, we used a spectral decomposition procedure derived from the approach of Schweitzer-Stenner and Bigman.[22]

$$A(\nu) = \nu[\sum_{j=0}^{N}\sum_{\rho=x,y} V_{j,\rho}(\nu)] \tag{3}$$

where the Voigtians $V_{i,\rho}(\nu)$ are given by

$$V_{j,\rho}(\tilde{\nu}) = \frac{1}{\pi}\frac{I_{j,\rho}\Gamma}{(\tilde{\nu}-\tilde{\nu}_{j,\rho})^2+\Gamma^2} \otimes \frac{1}{\sqrt{2\pi}\sigma}\exp[-\tilde{\nu}^2/(2\sigma^2)] \tag{4}$$

with $\tilde{\nu}_{j,y} = \tilde{\nu}_{j,x} + \Delta_j$, $\tilde{\nu}_{j,x} = \tilde{\nu}_{0,x} + \Omega_j$ and $\Omega_0 = 0$, the latter representing the Q_0-position. According to the above notation, $\tilde{\nu}_{0x}$ is the peak wavenumber of the Q_{0x} band and Δ_j is the $x-y$ splitting of the jth vibronic replica.

We used Voigtians rather than simple Lorentzians to model the shape of the Q bands; this is required to account for a Gaussian broadening of the bands, brought about by static heterogeneity (conformational disorder) and/or by coupling with a bath of low-frequency modes.[4,5,34] As evident from eq 4, parameters describing homogeneous and inhomogeneous broadening (i.e., Γ and σ) have been assumed to be identical for the fundamental Q_0 band and for all the vibronic replicas. This assumption is necessary in order to avoid a large number of poorly defined parameters in the fitting procedure.

Wavenumbers of heme vibrations Ω_j contributing to the Q_v band were heuristically determined from the low-temperature absorption spectra. Table 1 lists all the splitting and relative intensity values obtained from the decomposition of the spectra in Figure 1. They reveal that the splitting values and even more, that the absorption ratios $R_j = A_{Q_y}(j)/A_{Q_x}(j)$ of the identified doublets are not always identical. The doublet of the vibronic band at Ω_6 shows significantly less splitting and less asymmetry than the Q_0-doublet. While the splitting of Ω_4 is similar to that of Q_0, the intensity ratios are remarkably different. This already demonstrates that a complete modeling of all band splittings and intensity ratios cannot be accomplished solely based on

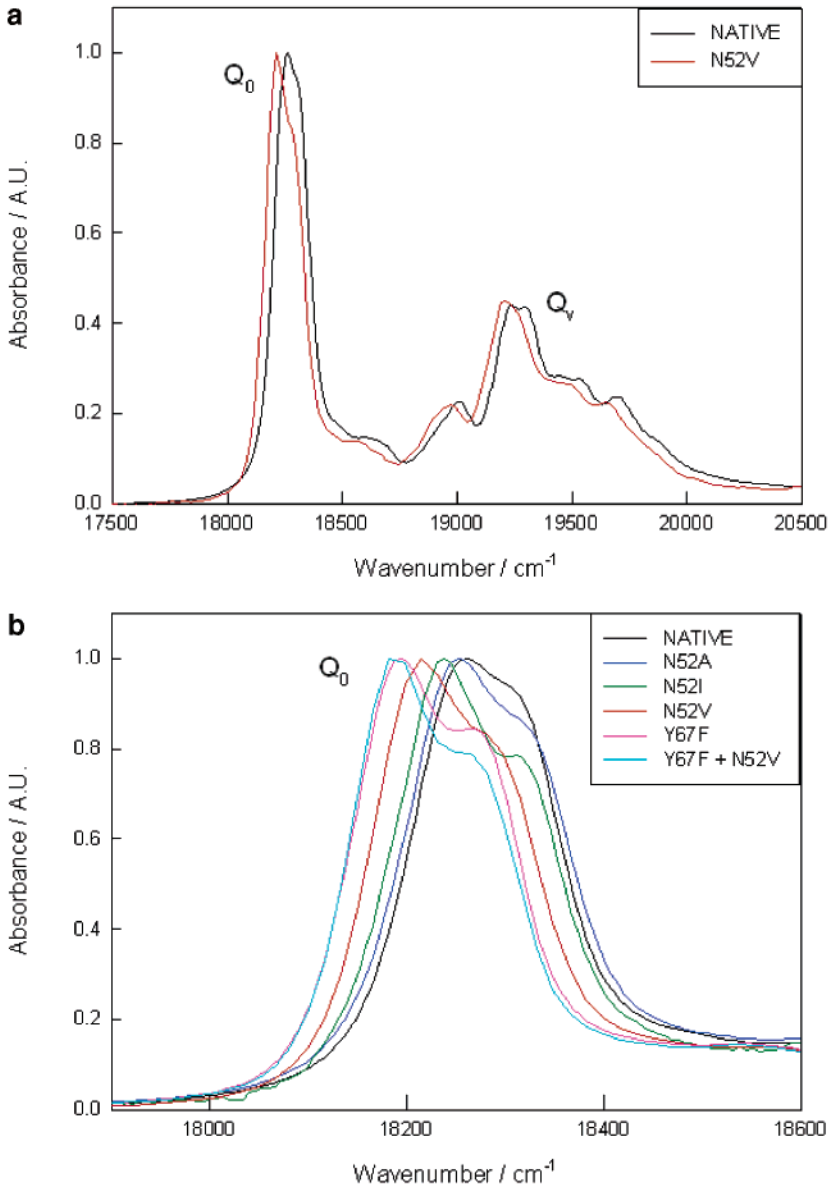

Figure 1. (a) Q_0 and Q_v band absorption spectra of yeast ferrocytochrome *c* and its mutant N52V; (b) Q_0-section of the absorption spectra of yeast ferrocytochrome *c* and its mutants N52V, N52A, N52I, Y67F, and N52VY67F. The spectra were taken at 20 K.

electronic perturbations. If they were dominant, all band splittings and intensity ratios would be identical.[22] Our analysis further reveals that both yeast cytochrome *c* Q_0-splitting and band asymmetry are significantly reduced compared with the respective values for horse heart, in agreement with findings reported by Vanderkooi and associates.[2] This suggests that heme perturbations in both proteins are substantially different.

As shown in ref 21, the relative intensities in the polarized resonance Raman spectra of yc in Figure 3 can be used to assign the above identified vibronic sideband contributions. The spectrum taken with 521 nm-excitation is dominated by bands from three A_{2g} modes, that is, 1581 cm^{-1} (ν_{19}), 1311 cm^{-1} (ν_{21}), and 1130 cm^{-1} (ν_{22}) and to a lesser extent by other bands assigned to three B_{1g} modes, that is 1619 cm^{-1} (ν_{10}), 1645 cm^{-1} (ν_{11}), and 749 cm^{-1} (ν_{15}). The spectrum obtained with 531 nm excitation additionally shows the strong resonance enhancement of ν_{15}. This results from the fact that the excitation wavelength is very close to the Q_v-resonance position of its resonance excitation profile. As argued by Levantino et al.,[21] a comparison of the absorptivity of the obtained Ω_j bands with the resonance Raman intensities obtained with Q_v-band excitation yielded the following assignments: Ω_4 to ν_{15}, Ω_6 to ν_{22}, Ω_8 to ν_{21}, and Ω_9 to ν_{19}. The assignment of the weak bands at $\Omega_1-\Omega_3$, Ω_5, Ω_7, and Ω_{10} are less clear in that they are likely to be associated with more than a single vibration. Since their spectral parameters are rather uncertain, we did not consider these bands further in our simulations of the optical spectra. Our assignments imply that the Q_v band is predominantly governed by the strong Herzberg−Teller coupling of A_{2g}-type modes, in perfect agreement with the findings reported for metalloporphyrins in solution.[35] We used the vibronic theory described in ref 21 to simulate the observed band splittings and the absorption ratios $R_j = A_{Q_y}(j)/A_{Q_x}(j)$ in terms of the coupling parameters defined by eqs 1 and 2. Table 1 compares the theoretically and experimentally obtained values and shows that they are in very good agreement. The corresponding coupling parameter values are listed in Table 2. As expected, the electronic perturbation values obtained for all mutants investigated are larger than the value obtained for wild-type yc. The $\delta_{QB}^{B_{1g}}$ values for N52V, N52A, and N52VY67F are similar though not identical and only slightly smaller than the value obtained for hhc, whereas the

TABLE 1: Experimental (exptl) and Simulated (sim) Spectral Parameters of the Q_0- and Q_v-Band Region of Yeast Cytochrome *c* and Its Mutant N52A, N52V, N52I, Y67F, and N52VY67F[a]

	yc exptl	yc sim	N52A exptl	N52 sim	N52V exptl	N52V sim	N52I exptl	N52I sim	Y67F exptl	Y67F sim	N52V/Y67F exptl	N52V/Y67F sim	hh exptl	hh sim
Δ_0 [cm^{-1}]	77	86	89	94	96	99	94	95	95	90	96	99	116	110
R_{Qx0}/R_{Qy0}	0.91	0.8	0.69	0.68	0.67	0.67	0.65	0.65	0.74	0.74	0.66	0.67	0.67	0.65
$\Delta(\nu_{15})$ [cm^{-1}]	77	71	89	87	94	94	94	96	95	97	96	98	116	114
$R_{Qx}(\nu_{15})/R_{Qy}(\nu_{15})$	1.71	1.73	1.76	1.75	1.1	1.1	1.39	1.38	1.5	1.51	1.34	1.34	1.37	1.33
$A_Q(\nu_{15})/A_{Q_0}$	0.16	0.16	0.19	0.19	0.19	0.19	0.17	0.17	0.19	0.19	0.19	0.18	0.17	0.16
$\Delta(\nu_{22})$ [cm^{-1}]	87	88	90	90	89	89	80	79	92	90	91	93	85	82
$R_{Qx}(\nu_{22})/R_{Qy}(\nu_{22})$	0.94	0.95	0.86	0.86	0.99	0.98	0.76	0.75	0.93	0.94	0.95	0.94	0.94	0.88
$A_Q(\nu_{22})/A_{Q_0}$	0.39	0.39	0.40	0.39	0.39	0.37	0.36	0.36	0.39	0.37	0.39	0.37	0.29	0.30
$\Delta(\nu_{21})$ [cm^{-1}]	776	75	89	89	94	95	94	94	95	95	96	96	116	107
$R_{Qx}(\nu_{21})/R_{Qy}(\nu_{21})$	1.54	1.56	1.22	1.21	1.39	1.4	1.12	1.19	1.15	1.15	1.14	1.15	1.0	0.92
$A_Q(\nu_{21})/A_{Q_0}$	0.18	0.17	0.20	0.21	0.21	0.21	0.21	0.21	0.22	0.21	0.21	0.21	0.23	0.22
$\Delta(\nu_{19})$ [cm^{-1}]	77	76	89	88	94	98	94	0.94	95	95	96	98	116	113
$R_{Qx}(\nu_{19})/R_{Qy}(\nu_{19})$	0.89	0.90	1.05	1.04	0.54	0.54	0.77	0.77	0.55	0.53	0.54	0.54	0.55	0.53
$A_Q(\nu_{19})/A_{Q_0}$	0.14	0.14	0.17	0.16	0.16	0.16	0.16	0.16	0.17	0.16	0.16	0.16	0.16	0.16

[a] Δ_0 is the splitting of the Q_0 band and $\delta(j)$ that of the *j*th vibronic band, R_{Qx0} and R_{Qy0} are the dipole strengths for the polarization directions *x* and *y* of the Q_0 transition, $R_{Qx}(j)$ and $R_{Qy}(j)$ are the dipole strengths for the polarization directions *x* and *y* of the vibronic side band assignable to vibration *j*, and A_{Q0} (A_Q *(j)*) denotes the absorptivity of the entire Q_0 band (vibronic sideband assignable to the *j*th vibration). The parameters were obtained from the spectra in Figure 1. The simulated values were obtained with the parameters listed in Table 2. The parameter values for horse heart cytochrome *c* have been added for comparison.[21]

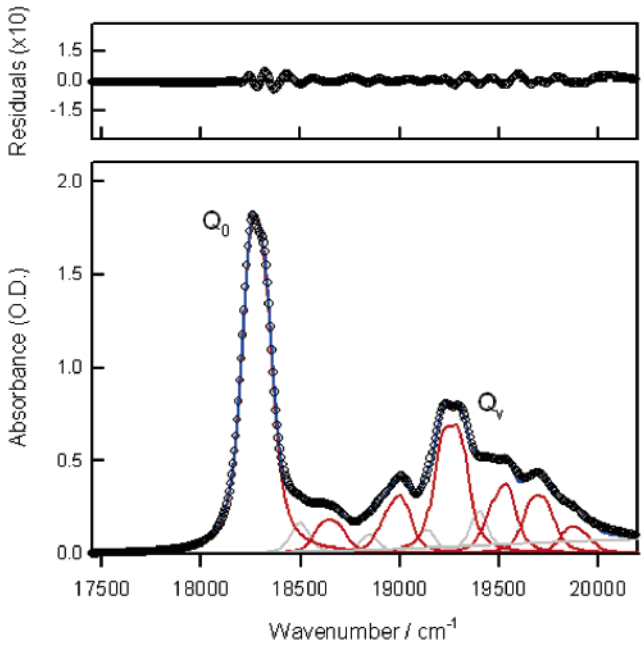

Figure 2. Spectral decomposition of the Q_0 and Q_v band region of yeast cytochrome *c* measured at 20 K by Voigtian band profiles described in Results and Discussion (taken from ref 21). The small circles depict the experimental data, lines represent the Voigtian components (red and gray) and the overall calculated band profile (blue). The residuals are shown on an expanded scale in the upper panel.

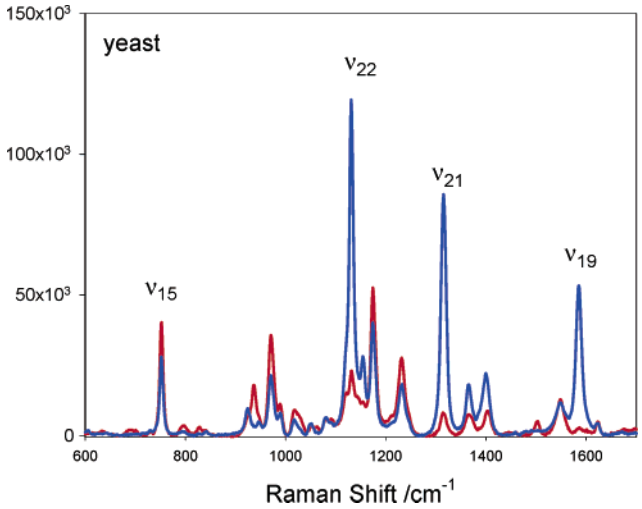

Figure 3. Polarized Raman spectra of yeast cytochrome *c* acquired with 521 nm (Q_v) excitation (red line, *x*-polarization parallel to the polarization of laser excitation; blue line, *y*-polarization perpendicular to the polarization of laser excitation). The spectra were taken at room temperature. The experimental methods and conditions are described in Material and Methods.

$\delta_{QB}^{B_{1g}}$ parameter observed for N52I is even slightly larger than that of hhc. As for the Y67F mutation, its $\delta_{QB}^{B_{1g}}$ value lies between that of hhc and yc. In our earlier paper, we interpreted the electronic perturbation as being related to the quadrupole energy term of the internal electric field as derived by Manas et al.[2] This term reflects the difference between the field gradients along the *x* and *y* directions, which correspond to the N−Fe−N axes of the heme group. Thus, it reflects the inhomogeneity of the electric field at the heme, and our data therefore suggest that this inhomogeneity increases for all the investigated yc mutations.

To briefly discuss the vibronic coupling parameters listed in Table 2, we confine ourselves to the $c_{QQ}^{A_{1g}}$ parameters of the A_{2g}-type modes ν_{19}, ν_{20}, and ν_{21}. As argued by Levantino et al.,[21] they mostly reflect the combined influence of ruffling (B_{1u}) and saddling (B_{2u}) out-of-plane deformations. It should be noted that the absolute values of these parameters are most likely overestimated, since we neglected Herzberg−Teller coupling $c_{QB}^{A_{1g}}$ in order to reduce the number of unknown parameters. However, a comparison of the different mutants is still possible. Inspection of the values in Table 2 reveals that the investigated mutations decrease $c_{QQ}^{A_{1g}}$ which indicates a reduced nonplanarity of the heme (only the $c_{QQ}^{A_{1g}}$ remains unaffected for Y67F) for all mutants investigated. Concerning the single mutations, one infers the following nonplanarity hierarchy: wild-type yc > N52A > N52V, N52I > Y67F. Within the limit of accuracy the double mutant N52VY67F cannot be distinguished from N52V. Interestingly, the leading Herzberg−Teller coupling parameters $c_{QB}^{A_{1g}}$ of ν_{19} and ν_{21} of all mutants are slightly larger than the values obtained for natural yc. This might indicate differences in the in-plane symmetric A_{1g} deformation, which can be described either as a contraction or an expansion of the heme core. Again, all these differences between the coupling parameters of wild-type yc and the mutants are consistent in that they

TABLE 2: Electronic and Vibronic Parameters Used to Obtain the Simulated Spectral Parameters Listed in Table 1

	yc	N52A	N52V	N52I	Y67F	N52V/Y67F
$\delta_{QB}^{B_{1g}}$ [cm^{-1}]	50	88	90	98	70	90
$\delta_{QB}^{B_{1g}}$ (ν_{15}) [cm^{-1}]	254[a]	276	276	261	276	276
$c_{QQ}^{B_{1g}}$ (ν_{15}) [cm^{-1}]	47	51	51	48	51	51
$c_{QB}^{A_{1g}}$ (ν_{15}) [cm^{-1}]	156	125	125	130	185	145
$c_{QQ}^{B_{1g}}$ (ν_{15}) [cm^{-1}]	200	172	138	170	222	172
$c_{QB}^{A_{2g}}$ (ν_{15}) [cm^{-1}]	60	65	65	61	65	65
$c_{QB}^{A_{2g}}$ (ν_{22}) [cm^{-1}]	500[a]	500	500	462	500	500
$c_{QB}^{B_{2g}}$ (ν_{22}) [cm^{-1}]	60	37	35	20	55	40
$c_{QQ}^{A_{1g}}$ (ν_{22}) [cm^{-1}]	65	23	40	−18	50	40
$c_{QB}^{A_{2g}}$ (ν_{21}) [cm^{-1}]	300[a]	350	350	350	350	350
$c_{QB}^{B_{2g}}$ (ν_{21}) [cm^{-1}]	76	50	60	50	80	60
$c_{QQ}^{A_{1g}}$ (ν_{21}) [cm^{-1}]	160	122	130	130	160	130
$c_{QB}^{A_{2g}}$ (ν_{19}) [cm^{-1}]	270[a]	290	290	290	290	290
$c_{QB}^{B_{2g}}$ (ν_{19}) [cm^{-1}]	87	60	77	60	95	77
$c_{QQ}^{A_{1g}}$ (ν_{19}) [cm^{-1}]	150	120	60	82	90	60

[a] Vibronic coupling term in D_{4h} symmetry.

TABLE 3: Out-of-Plane Deformations (in Å) along the Lowest Frequency Normal Coordinates (Minimal Basis Set) of the Hemes Extracted from the Yeast Ferrocytochrome *c* Models after 1 ns of Molecular Dynamics Simulation

model	D_{oop}[a]	sad B_{2u}	ruf B_{1u}	dom A_{2u}	wav(x) $E_{g(x)}$	wav(y) $E_{g(y)}$	pro A_{1u}
yeast c	0.9838	0.132	0.927	−0.087	−0.034	−0.237	0.116
N52V	0.6892	0.040	0.677	−0.016	0.028	−0.094	0.001
N52vY67F	0.7714	−0.132	0.742	0.054	0.008	−0.134	0.048

[a] Total distortions using the extended basis set: see Jentzen et al. (19) for details.

indicate that the mutations makes the protein more similar to hhc.

To further validate our interpretation of the vibronic coupling parameters we performed a 1 ns MD simulation for two representative mutants, that is, N52V and N52VY67F. The NSD calculations performed on the respective hemes extracted from these simulations yielded the out-of-plane deformations listed in Table 3, which clearly support the conclusion drawn from the vibronic analysis of the optical spectra. The N52V and N52VY67F mutants both indicate a more planar heme when compared to the wild-type heme with total oop distortions of 0.6892 and 0.7714 Å for N52V and N52VY67F, respectively, compared to 0.9838 Å for the wild-type heme. Ruffling (B_{1u}) in both N52V and N52VY67F is also lowered when compared to the wild-type (0.677 and 0.742 Å for the mutants vs 0.927 Å for wild-type). Saddling is also reduced for N52V when compared to the wild-type and of opposite sign for N52VY67F.

The question now arises as to whether the observed perturbations and deformations are of functional significance. The study of Blouin and Wallace clearly revealed that the investigated mutations significantly affect the redox potential by changing the respective enthalpy and entropy contributions.[23] The authors focused their discussion on how the presence of water molecules in the heme cavity is affected by the mutations. They analyzed the temperature dependence of the equilibrium between reduced and oxidized forms of the mutants and found competing enthalpy and entropy contributions to E_m^0. The latter clearly favors the oxidized and the former stabilizes the reduced state. Figure 4 exhibits the relationship between the $\Delta\Delta H_{red,i} = \Delta H_{red,i} - \Delta H_{red,yc}$, values and $\delta_{QB}^{B_{1g}}$ for yc and the mutants i investigated

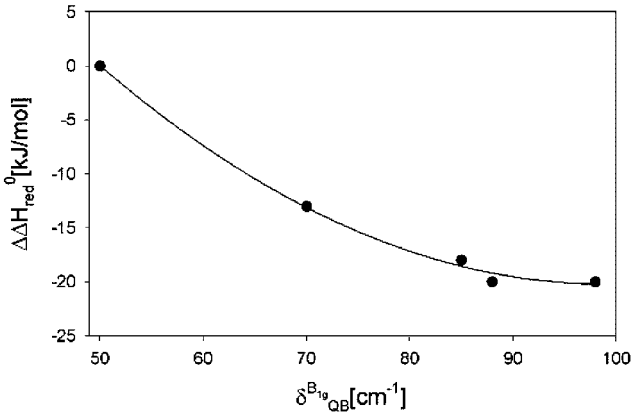

Figure 4. $\Delta\Delta H_{red}$ of yc and its mutants N52A, N52V, N52I, and Y67F as a function of the electronic perturbation parameter $\delta_{QB}^{B_{1g}}$. The solid line results from an empirical fit of a quadratic function to the experimental data.

in the present study. Apparently, an increase in $\delta_{QB}^{B_{1g}}$ correlates well with a concomitant decrease of the (negative) $\Delta\Delta H_{red,i}$ value. The depicted correlation is reproduced very well by a quadratic equation which makes sense since any perturbation of energy levels would scale with the square of the perturbing potential in second-order Rayleigh−Schrödinger perturbation theory. The plot does not contain N52FY67F, for which the thermodynamic behavior is very different from that of the single mutants. This mutant is discussed in more detail below.

To develop a possible rationale for the correlation between $\delta_{QB}^{B_{1g}}$ and $\Delta\Delta H_{red}$, we first invoke the fact that Blouin and Wallace have clearly shown that the investigated mutations perturb the network of water molecules in the heme pocket.[23] This decreases the effective dielectric constant and thus the field and most likely also the electric field gradient. In fact, the reduced inhomogeneity of the field in yc compared with hhc correlates with a reduced electric field strength at the heme position.[4] Second, we have to consider how the inhomogeneity of the electric field can influence the ground state of the heme group and the energy hierarchy of the Fe orbitals. In this context, it must be emphasized that the splitting of the optical spectra reflects a perturbation of the 2-fold degenerate excited Q-state. The electric field itself cannot cause any distortion of the ground state of the undistorted D_{4h} symmetry, because this requires perturbations of A_{1g} symmetry.[22] However, if one assumes that the symmetry of the heme already deviates significantly from D_{4h} in the absence of an electric field because of heme protein interactions and peripheral substituents (a notion supported by the depolarization ratio dispersion of Raman bands[17,18]), the electric field can even directly affect the heme structure. Even if D_{4h} is still an appropriate reference symmetry, the vibronic perturbations described by the matrix elements $\langle g|\partial V^{B_{1g}}/\partial q_i^{B_{1g}}|g\rangle q_i^{B_{1g}}$, where $q_i^{B_{1g}}$ is the normal coordinate of the ith vibration exhibiting B_{1g} symmetry in D_{4h}, can give rise to ground-state deformations $\delta_i^{\bar{q}B_{1g}}$.[35] As shown earlier, deformations along the coordinates of the lowest frequency modes are predominant for a distinct symmetry block.[36,37] For B_{1g}, this corresponds to a rhombic deformation of the heme core, which increases the splitting of the ^1E level of the heme iron.[38] The electric field can directly cause additional splitting of ^1E via its B_{1g}-type quadrupole component as probed by $\delta_{QB}^{B_{1g}}$. All these B_{1g}-type perturbations (electric field and heme deformations) can further mix the ground state ($^1A_{1g}$) and one of the singlet excited states ($^1B_{1g}$). These interactions have in common that they stabilize the ground state ($^1A_{1g}$ or ^1E) and thus increase the ionization energy. However, a quantitative assessment of

the influence of electronic and vibronic perturbations on $\Delta\Delta H_{red}$ requires (a) a comparison of ferricytochrome and ferrocytochrome *c* and (b) an analysis of the ground-state heme deformations which can be accomplished by polarized resonance Raman dispersion spectroscopy. Both projects are currently pursued in our laboratory. To account for the $\Delta\Delta H_{red}$ variation reported by Blouin and Wallace,[23] the perturbation-induced stabilization energy of ferrocytochrome has to exceed that of the ferri state by 1200 cm^{-1}. This is a comparatively large coupling energy.

Our results further indicate a correlation between out-of-plane deformations and $\Delta\Delta H_{red}$. As shown by Safo et al.,[39] by means of structural and Mössbauer studies on low spin hexacoordinated Fe^{2+} and Fe^{3+} porphyrins, ruffling is likely to stabilize the oxidized over the reduced state in that it facilitates porphyrin $\rightarrow Fe^{3+}$ electron back-donation. Recently, Sun et al. arrived at a similar conclusion. They measured the electron-transfer properties of various fluorinated cobalt porphyrins, and their result led them to conclude that ruffling decreases porphyrin $\pi-$metal dπ interactions and minimizes the in-plane reorganization energy of the heme macrocycle associated with the iron oxidation.[40] Hence, a decrease in ruffling stabilizes the ferro state. As mentioned above, the coupling parameters inferred from our absorption data and our NSD calculations are consistent with a reduced ruffling in the mutated cytochromes, which moves the equilibrium in favor of the reduced state.

Apparently, one mutant, that is, N52VY67F, does not fit into the picture at all. Our data suggest that the second mutation (Y67F) has a negligible effect in the presence of N52V. The data of Blouin and Wallace argue to the contrary.[23] However, the thermodynamic parameters obtained for this mutant indicate that it is a special case. Blouin and Wallace hypothesized that the double mutation causes a more direct effect in that it eliminates the screening of the heme iron from the negatively charged heme propionate which is supposed to stabilize the ferri state. Resonance Raman data seem to indicate that the in-plane heme deformation is different for N52V and N52VY67F (Huang, Hagarman, Schweitzer-Stenner; unpublished). Furthermore, it is to be noted that our NSD results for N52VY67F show an inversion of the saddling deformation with respect to wild-type. Doubtless, further investigations are necessary to clarify this issue.

Taken together, our results unambiguously show that the mutations involving the replacement of polar by aliphatic side chains at positions 52 and 67 of yc increases the electronic B_{1g} perturbation at the heme plane which is likely to reflect the heterogeneity of the internal electric field. This causes a larger splitting of the Q- and Q_v bands in the optical spectrum. Concomitantly, the ruffling and saddling deformations of the functional heme group decrease. We argue that both effects contribute to the enthalpic part of the redox potential, which favors the reduced state.

Acknowledgment. We thank Bruce Stewart [Dalhousie University] for the expert expression and purification of the mutant cytochromes. Financial support was provided from a grant from the National Science Foundation (Grant MCB-0318749) and ACS-Petroleum Research Funds (PRF Grant 37406-A.C.) to R.S.S. and from the Natural Sciences and Engineering Research Council of Canada to C.W.

References and Notes

(1) Warshel, A. *Proc. Natl. Acad. Sci. U.S.A.* **1977**, *74*, 1789.

(2) Manas, E. S.; Vanderkooi, J. M.; Sharp, K. A. *J. Phys. Chem. B* **1999**, *103*, 6344.

(3) Manas, E. S.; Wright, W. W.; Sharp, K. A. Friedrich, J.; Vanderkooi, J. M. *J. Phys. Chem. B* **2000**, *104*, 6932−6941.

(4) Laberge, M.; Köhler, M.; Vanderkooi, J. M.; Friedrich, J. *Biophys. J.* **1999**, *77*, 3293.

(5) Prabhu, N. V.; Dalosto, S. D.; Sharp, K. A.; Wright, W. W.; Vanderkooi, J. M. *J. Phys. Chem. B* **2002**, *106*, 5561.

(6) Laberge, M. *Biochim. Biophys. Acta* **1998**, *1386*, 305.

(7) Stryer, L. *Biochemistry;* W. H. Freeman & Co.: New York, 2002.

(8) Chin, J. K.; Jimenez, R.; Romesberg, F. E. *J. Am. Chem. Soc.* **2002**, *124*, 1846.

(9) Grunner, M. R.; Honig, B. *Proc. Natl. Acad. Sci. U.S.A.* **1991**, *88*, 9151.

(10) Muegge, I.; Qi, P. X.; Wand, A. J.; Chu, Z. T., Warshel, A. *J. Phys. Chem. B* **1997**, *101*, 825.

(11) Sharp, K. A. Calculation of Electron-Transfer Reorganization Energies Using the Finite Difference Poisson−Boltzmann Model. *Biophys. J.* **1998**, *73*, 1241.

(12) Sutherland, J. C.; Klein, M. P. Magnetic Circular Dichroism of Cytochrome *c*. *J. Chem. Phys.* **1972**, *51*, 76−84.

(13) Friedman, J. M., Rousseau, D. L.; Adar, F. *Proc. Natl. Acad. Sci. U.S.A.* **1977**, *74*, 2607.

(14) Wagner, G. C.; Kassner, R. J. *Biochem. Biophys. Res. Commun.* **1975**, *63*, 385.

(15) Collins, D. W.; Fitchen, D. B.; Lewis, A. Resonance Raman Scattering from Cytochrome *c*: Frequency Dependence of Depolarization Ratio. *J. Chem. Phys.* **1973**, *59*, 5741.

(16) Zgierski, M. Z.; Pawlikowski, M. *Chem. Phys*. **1982**, *65*, 335.

(17) Bobinger, U.; Schweitzer-Stenner, R.; Dreybrodt, W. *J. Raman Spectrosc.* **1988**, 191−202.

(18) Schweitzer-Stenner, R.; Bobinger, U.; Dreybrodt, W. *J. Raman Spectrosc.* **1991**, *22*, 65.

(19) Jentzen, W.; Song, X. Z.; Shelnutt, J. A. *J. Phys. Chem. B* **1997**, *101*, 1684.

(20) Jentzen, W.; Ma, J.-G.; Shellnutt, J. A. *Biophys. J.* **1998**, *74*, 753.

(21) Levantino, M.; Huang, Q.; Cupane, A.; Laberge, M.; Hagarman, A.; Schweitzer-Stenner, R. *J. Chem. Phys.* **2005**, *123*, 054508.

(22) Schweitzer-Stenner, R.; Bigman, D. *J. Phys. Chem. B* **2001**, *105*, 7064.

(23) Blouin, C.; Wallace, C. J. A. *J. Biol. Chem.* **2001**, *276*, 28814.

(24) Berghuis, A. M.; Guillemette, J. G.; Smith, M.; Brayer, G. D. *J. Mol. Biol*. **1994**, *235*, 1326.

(25) Gouterman, M. *J. Chem. Phys.* **1959**, *30*, 1139.

(26) Canter, G. W. *J. Chem. Phys.* **1981**, *74*, 157.

(27) Parrish, J. C.; Guillemette, J. G.; Wallace, C. J. A. *Biochem. Cell. Biol*. **2001**, *79*, 83−91.

(28) Wallace, C. J. A.; Clark-Lewis, I. *Biochem. Cell Biol.* **2000**, *78*, 79.

(29) Laskowski, R. A.; MacArthur, M. W.; Moss, D. S.; Thornton, J. M. *J. Appl. Crystallogr*. **1993**, *26*, 283.

(30) Brooks, B. R.; Bruccoleri, R. E.; Olafson, B. D.; States, D. J.; Swaminathan, S.; Karplus, M. CHARMM: A program for macromolecular energy, minimization and dynamics calculations. *J. Comput. Chem.* **1983**, *4*, 187−217.

(31) Authenrieth, F.; Tajkhorshid, E.; Baudry, J.; Luthey-Schulten Z. *J. Comput. Chem.* **2004**, *25*, 1613.

(32) Christian, J. F.; Unni, M.; Sage, J. T.; Champion, P. M. *Biochemistry* **1997**, *36*, 11198−11204.

(33) Cupane, A., Leone, M.; Militello, V.; Friedman, F. K.; Koley, A. P.; Vasquez, G. B.; Brinigar, W. S.; Karavitis, M.; Fronticelli, C. *J. Biol. Chem.* **1997**, *272*, 26271.

(34) Cupane, A. S.; Leone, M.; Vitrano, E.; Cordone, L. *Eur. Biophys. J.* **1995**, *23*, 385.

(35) Schweitzer-Stenner, R.; Stichternath, A.; Dreybrodt, W.; Jentzen, W.; Song, X.-Z.; Shelnutt, J. A.; Faurskov Nielsen, O.; Medforth, C. J.; Smith, K. M. *J. Chem. Phys.* **1997**, *107*, 1794.

(36) Huang, Q.; Szigetti, K.; Fidy, J.; Schweitzer-Stenner, R. *J. Phys. Chem. B* **2003**, *107*, 2822.

(37) Huang, Q.; Medforth, C.; Schweitzer-Stenner, R. *J. Phys. Chem. A* **2005**, *109*, 10493.

(38) Mayer, A.; Eicher, H. *J. Mol. Catal.* **1984**, *23*, 151.

(39) Safo, M. K.; Nesset, M. J. M.; Walker, F. A.; Debrunner, P. G.; Scheidt, W. R. *J. Am. Chem. Soc.* **1997**, *119*, 9438.

(40) Sun, H.; Smirnov, V. V.; DiMagno, S. G. *Inorg. Chem.* **2003**, *42*, 6023.